Electronic Supplementary Information (ESI)

Enhanced in-plane thermal conductivity of polyimide-based composites via in-situ interfacial modification of graphene

Huiya Lan, Bin Wu *, Yuye Yan, Ru Xia*, Jiasheng Qian

Key Laboratory of Environment-Friendly Polymeric Materials of Anhui Province, School of Chemistry & Chemical Engineering, Anhui University, Hefei, Anhui, 230601, China

Contents:

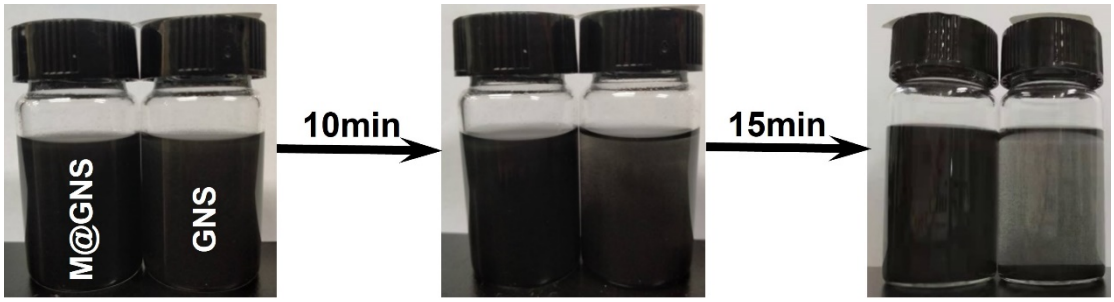

Fig. S1. Dispersion of GNS and M@GNS in H_2O for 15 minutes.

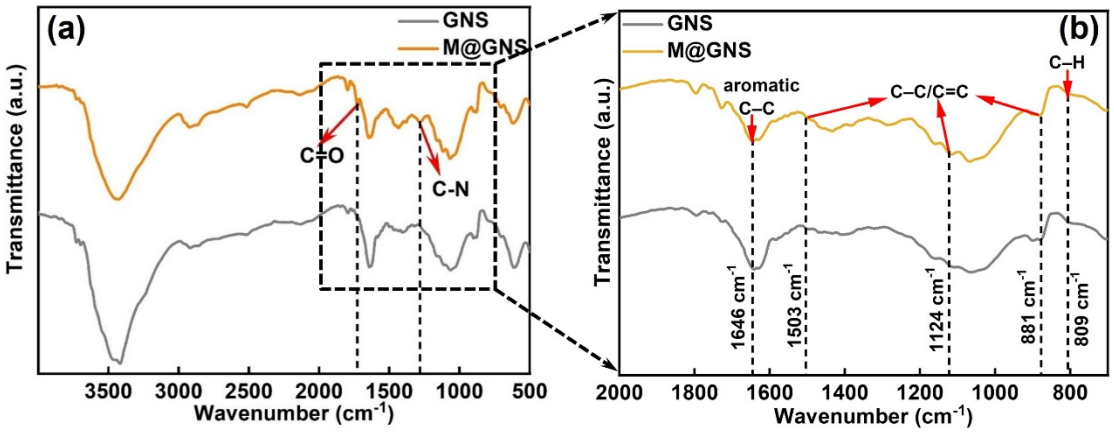

Fig. S2. The FT-IR of GNS and M@GNS, respectively.

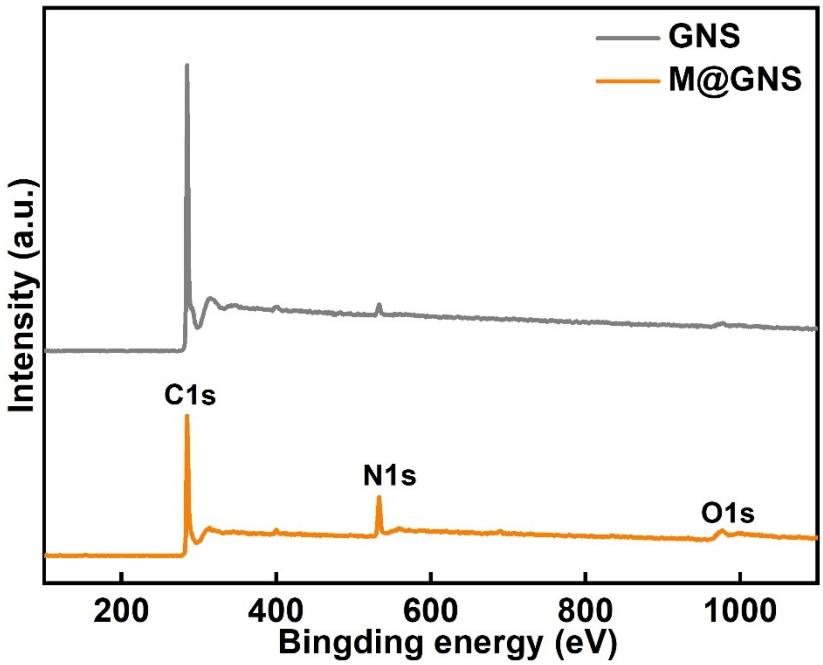

Fig. S3. The XPS full spectra of GNS and M@GNS, respectively.

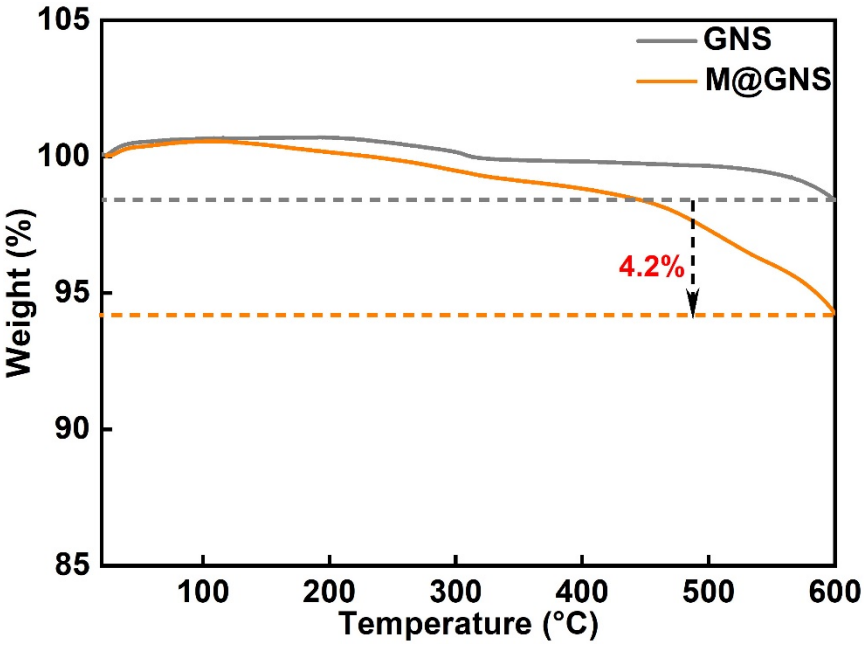

Fig. S4. The TGA of GNS and M@GNS, respectively.

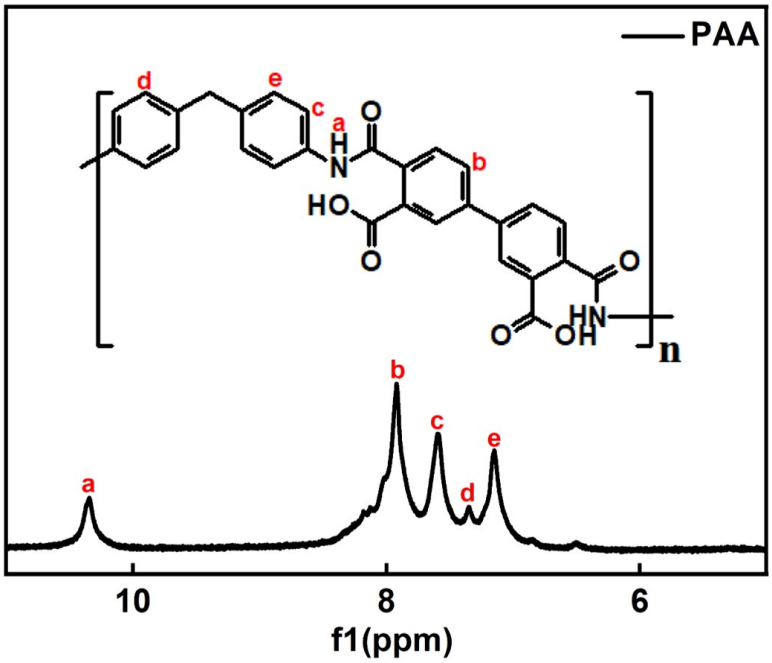

Fig. S5. The ^{1}H NMR of PAA.

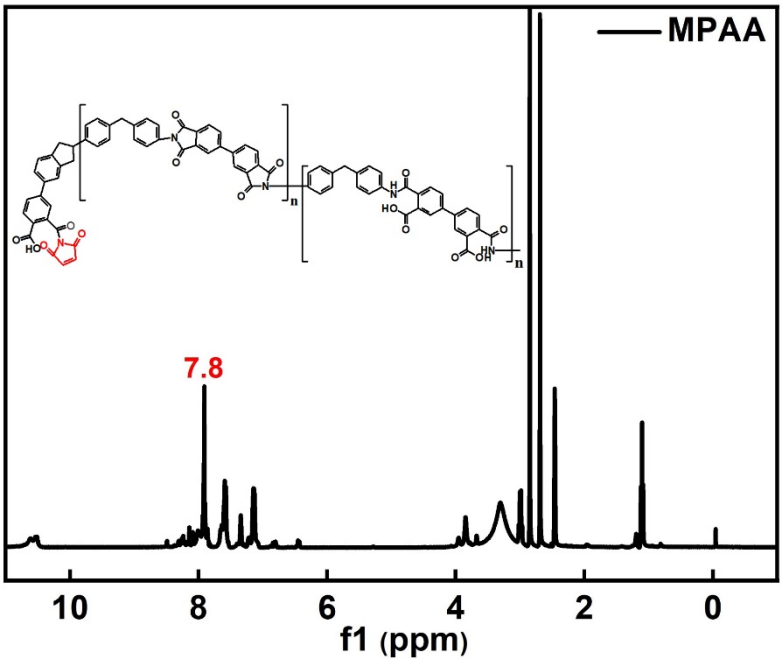

Fig. S6. The ^{1}H NMR of MPAA.

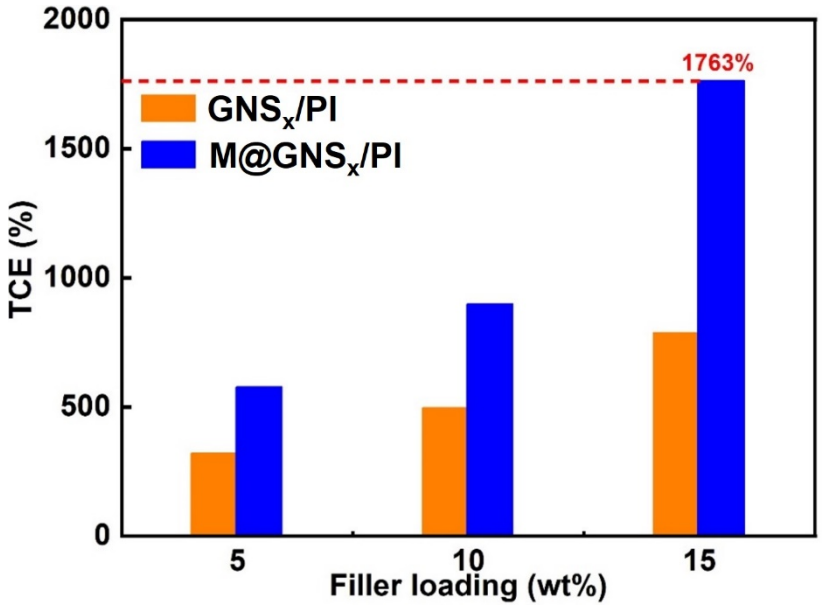

Fig.S7. TCE of M@GNS$_x$/PI and GNS$_x$/PI with different filler loading.

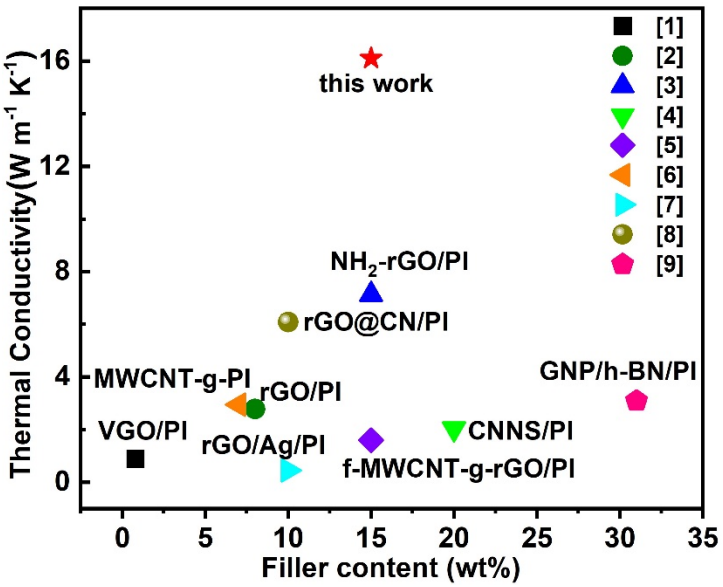

Fig.S8. M@GNS_{15}/PI comparison of thermal conductivity with the literature values[1-9].

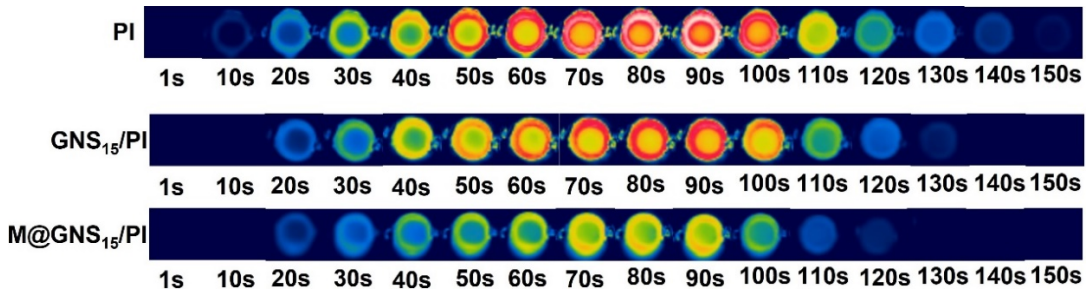

Fig. S9. Infrared thermal images of PI, GNS_{15}/PI, and M@GNS_{15}/PI in the process of LED lamp power-on to power-off.

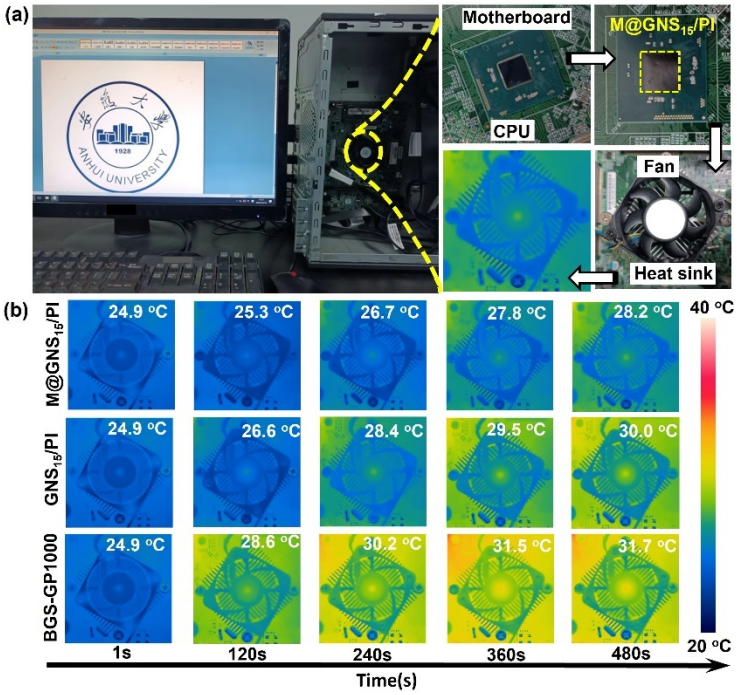

Fig. S10. (a) Experimental setup and the schematic configuration for comparing the cooling efficiency between M@GNS_{15}/PI, GNS_{15}/PI, and BGS-GP1000 based on desktop computer systems. (b) Comparative infrared thermal images of the motherboard when M@GNS_{15}/PI, GNS_{15}/PI, and BGS-GP1000 were used as heat dissipation materials as a function of running time, respectively.

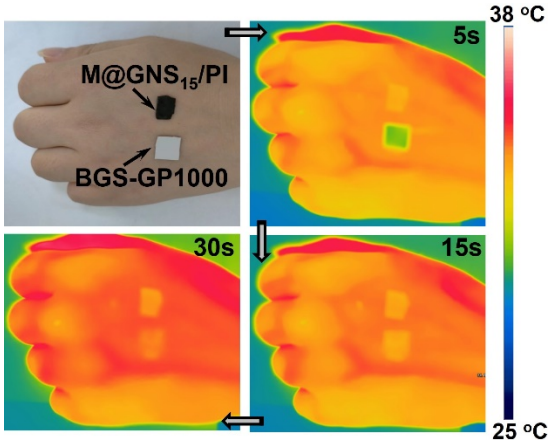

Fig. S11. Photograph and infrared thermal image of BGS-GP1000 and M@GNS_{15}/PI placed on the skin at different time.

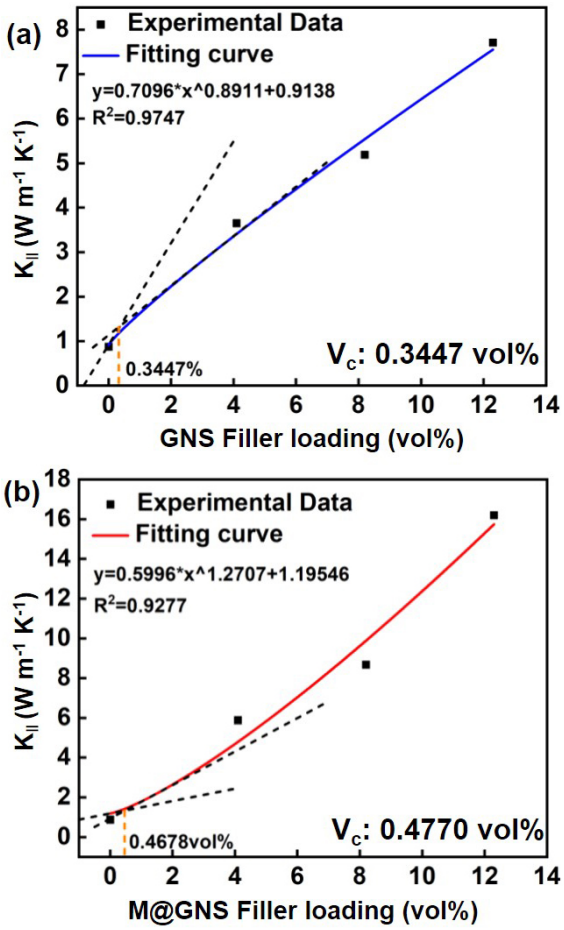

Fig. S12. V_c achieved by tangential process of experimental data for (a) GNS and (b) M@GNS.

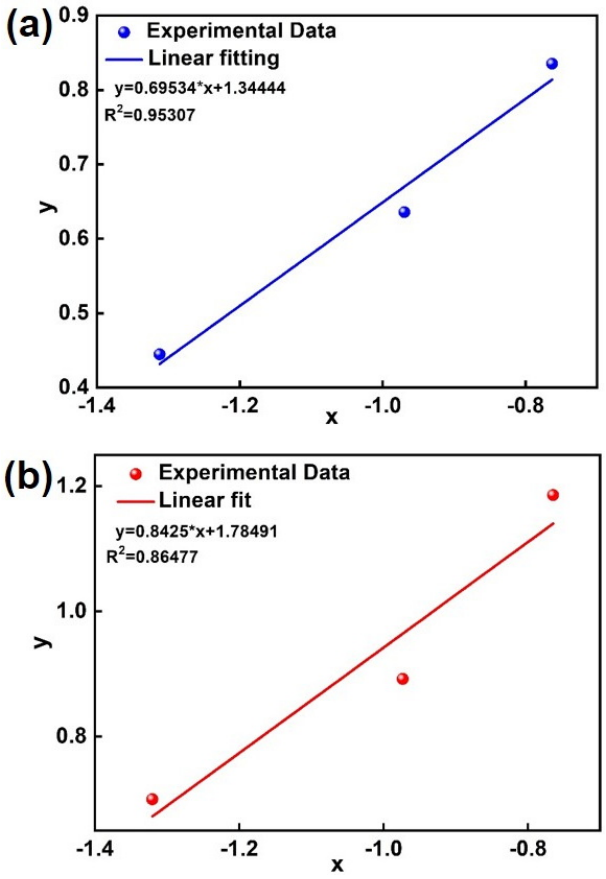

Fig. S13. The fitting process of Foygel model for (a) GNS_{15}/PI, and (b) M@GNS_{15}/PI, respectively.

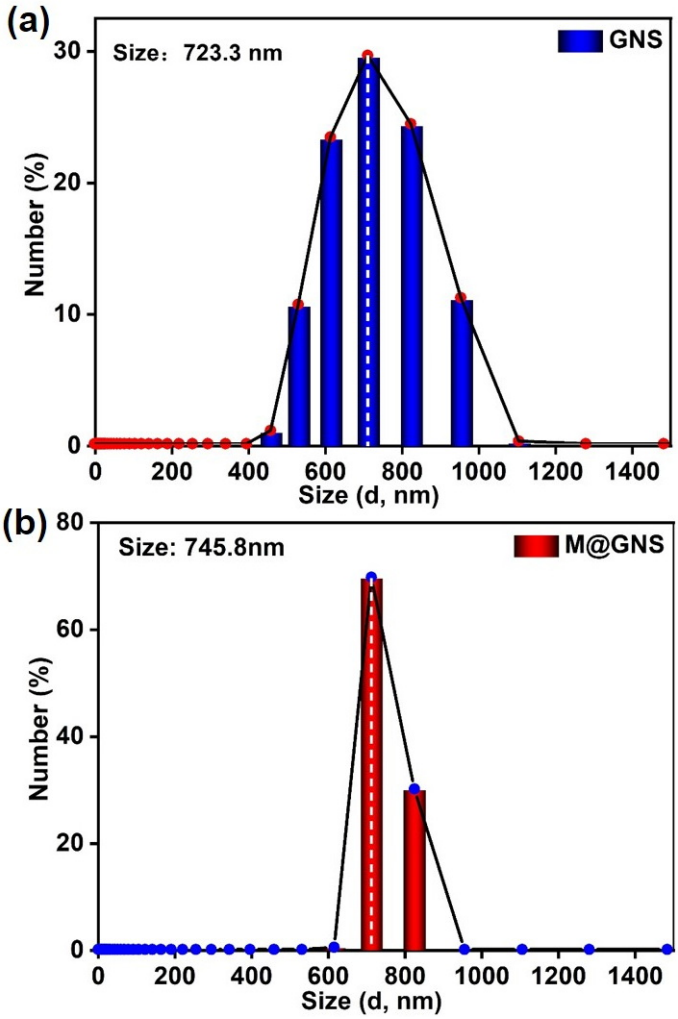

Fig. S14. The distribution of sheet size of GNS and M@GNS obtained by dynamic light scattering, respectively.

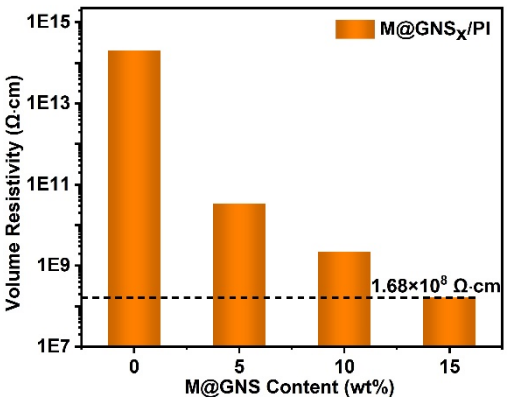

Fig. S15. Volume resistivities of the M@GNS$_x$/PI with different filler loading.

The wt% of M@GNS in composite ($wt\%_{(M@GNS)}$) was obtained by the following equation:

$$wt\%_{(M@GNS)} = m_{(M@GNS)}/m_{(M@GNSx/PI)} \times 100\% \quad (1)$$

where $m_{(M@GNS)}$ and $m_{(M@GNSx/PI)}$ represented the weight of M@GNS and M@GNS$_x$/PI, respectively.

To calculate volume fraction (vol%) of M@GNS in composite ($vol\%_{(M@GNS)}$), we have transformed the formula as follows:

$$\begin{aligned} vol\%_{(M@GNS)} &= V_{(M@GNS)}/V_{(M@GNSx/PI)} \times 100\% \\ &= (m_{(M@GNS)}/\rho_{(M@GNS)})/(m_{(M@GNSx/PI)}/\rho_{(M@GNSx/PI)}) \times 100\% \\ &= (m_{(M@GNS)}/m_{(M@GNSx/PI)})/(\rho_{(M@GNSx/PI)}/\rho_{(M@GNS)}) \times 100\% \\ &= wt\%_{(M@GNS)} \times (\rho_{(M@GNSx/PI)}/\rho_{(M@GNS)}) \quad (2) \end{aligned}$$

where $V_{(M@GNS)}$ and $V_{(M@GNS/PI)}$ was denoted the volume of M@GNS and M@GNS$_x$/PI, respectively. $\rho_{(M@GNS)}$ represented the density of M@GNS, which was achieved by density balance. $\rho_{(M@GNS/PI)}$ was got by the following formula.

$$\rho_{(M@GNS/PI)} = m_{(M@GNS/PI)}/V_{(M@GNS/PI)} \quad (3)$$

As GNS was the main thermal conductivity filler, analyzing the contact thermal resistance (R_c) between GNS layers in detail before and after maleimide modification is necessary. The nonlinear model proposed by Foygel et al. to calculate the contact thermal resistance. The model is given by the following equations.

$$K_c\text{-}K_{PI} = \kappa_0[(V_f\text{-}\ V_c)/(1\text{-}\ V_c)]^{\tau} \quad (4)$$

where K_c and K_{PI} are the thermal conductivity of the M@GNS/PI (or GNS/PI) with different filler loading and PI, respectively; κ_0 is a pre-exponential factor ratio that is the expected contribution of filler; V_f represents the volume fraction of fillers in composites; V_c is the critical volume content of filler (fitted from a tangent progression of the experimental data), respectively.

As depicted in Fig. S9, the V_c values are 0.389 vol % and 0.477 vol % for the GNS/PI and M@GNS/PI, respectively. τ is a conductivity exponent dependent on the aspect ratio of filler.

To calculate the R_c between filler, we have transformed the Foygel model formula as follows.

$$K_c\text{-}K_{PI} = \kappa_0[(V_f\text{-}\ V_c)/(1\text{-}\ V_c)]^{\tau} \quad (5)$$

$$\lg(K_c\text{-}K_{PI}) = \lg\{\kappa_0[(V_f\text{-}\ V_c)/(1\text{-}\ V_c)]^{\tau}\} \quad (6)$$

$$\lg(K_c\text{-}K_{PI}) = \lg\kappa_{0\,+}\,\tau\lg[(V_f\text{-}\ V_c)/(1\ \text{-}\ V_c)] \quad (7)$$

The formula can be simplified as:

$$y=a+bx \quad (8)$$

where y equals $\lg(K_c\text{-}K_{PI})$; x equal $\lg[(V_f\text{-}\ V_c)/(1\ \text{-}\ V_c)]$; a equals $\lg k_0$ and b equals τ. As shown in Fig.S10, the slope and intercept of the fitted line correspond to τ and $\lg k_0$. And the calculated k_0 and τ of GNS/PI and M@GNS/PI were exhibited in Table S3.

The contact resistance (R) between GNS layers or between M@GNS can be found according to the equation.

$$R = 1/(\kappa_0 L V_c^{\tau}) \quad (9)$$

where L is the sheet size of the filler, The distribution of M@GNS and GNS sheet size was obtained by dynamic light scattering in Fig. S11. The mean sheet size of M@GNS and GNS was 745.8 nm and 723.3 nm, respectively. The calculated R values are 1.08×10^{6} K W^{-1} and 1.31×10^{8} K W^{-1} for the M@GNS_{15} /PI and GNS_{15}/PI, respectively.

The contact thermal resistance (R_c) between M@GNS (or GNS) was obtained by following the equation.

$$R_c=R\times S_c \quad (10)$$

$$S_c=\pi/100\times(L/2)^2 \quad (11)$$

where S_c is the average overlap area between M@GNS (or GNS), considering the reassembly of M@GNS (or GNS) during the coating process, it is more proper to calculate S_c using the size of 2D nanofillers in the composites. It can be assumed that 1/100 of each M@GNS (or GNS) is involved in the heat conduction of the network. Therefore, S_c of M@GNS and GNS was 4.37×10^{-15} m^2 and 4.11×10^{-15} m^2, respectively.

Table S1. The weight fraction and volume fraction of fillers in the M@GNS_x/PI.

Sample	wt %	vol%
M@GNS_5/PI	5	4.1
M@GNS_{10}/PI	10	8.2
M@GNS_{15}/PI	15	12.3

Table S2. Comparison of atomic concentration of C, N, and O in GNS and M@GNS by the XPS full spectrums.

Samples	Atomic concentration%			C/N	C/O
	C 1s	N 1s	O 1s	atomic ration	atomic ration
GNS	96.56	1.44	2.00	67.06	48.28
M@GNS	85.01	2.52	11.54	33.73	7.37

Table S3. k_0 and τ in Foygel model for GNS_{15}/PI and M@GNS_{15}/PI.

Sample	k_0(W/m K)	τ
GNS_{15}/PI	22.1	0.70
M@GNS_{15}/PI	60.9	0.84

Table S4. The capability parameter of the model system.

Materials	P (g cm^{-3})	C_p (J g^{-1} K^{-1})	$\lambda_{\parallel}$ (W m^{-1} K^{-1})
GNS_{15}/PI	1.29	1.23	7.713
M@GNS_{15}/PI	1.23	1.29	16.10
PI matrix	1.39	1.00	0.870

Table S5. The geometric parameter of the model system.

Models	Length(mm)	Width(mm)	Height(mm)
GNS_{15}/PI	25	25	0.06
M@GNS_{15}/PI	25	25	0.06
PI matrix	25	25	0.06

Reference：

1. S. Fazil, S. Saeed, M. Waseem, W. Rehman, M. Bangesh and K. Liaqat, *Polym. Composite*, 2018, **39**, E1635-E1642.
2. S. Wei, Q. Yu, Z. Fan, S. Liu, Z. Chi, X. Chen, Y. Zhang and J. Xu, *RSC Adv.*, 2018, **8**, 22169-22176.
3. K. Ruan, Y. Guo, C. Lu, X. Shi, T. Ma, Y. Zhang, J. Kong and J. Gu, *Research (Wash D C)*, 2021, **2021**, 8438614.
4. Y. Wang, X. Zhang, X. Ding, P. Zhang, M. Shu, Q. Zhang, Y. Gong, K. Zheng and X. Tian, *Compos. Part B-Eng.*, 2020, **199**, 108267.
5. Y. Guo, K. Ruan, X. Yang, T. Ma, J. Kong, N. Wu, J. Zhang, J. Gu and Z. Guo, *J. Mater. Chem. C*, 2019, **7**, 7035-7044.
6. C. Wang, B. Cong, J. Zhao, X. Zhao, D. Wang, H. Zhou and C. Chen, *RSC Adv*, 2020, **10**, 13517-13524.
7. Y. Guo, X. Yang, K. Ruan, J. Kong, M. Dong, J. Zhang, J. Gu and Z. Guo, *ACS Appl. Mater. Interfaces*, 2019, **11**, 25465-25473.
8. Y. Wang, X. Zhang, X. Ding, Y. Li, P. Zhang, M. Shu, Q. Zhang, Y. Gong, K. Zheng, B. Wu and X. Tian, *Compos. Sci. Technol.*, 2021, **205**, 108693.
9. R. Li, C. Ding, J. Yu, X. Wang and P. Huang, *High Perform. Polym.*, 2021, **33**, 905-913.